J. Fluid Mech. (1998), *vol.* 355, *pp.* 139–162. Printed in the United Kingdom

On the stability of large-amplitude vortices in a continuously stratified fluid on the *f*-plane

By E. S. BENILOV[1]†, D. BROUTMAN[2] AND E. P. KUZNETSOVA[1]

[1] Department of Mathematics, University of Tasmania, PO Box 1214, Launceston 7250, Australia

[2] School of Mathematics, University of New South Wales, Sydney 2052, Australia

(Received 22 June 1995 and in revised form 27 August 1997)

The stability of continuously stratified vortices with large displacement of isopycnal surfaces on the *f*-plane is examined both analytically and numerically. Using an appropriate asymptotic set of equations, we demonstrated that sufficiently large vortices (i.e. those with small values of the Rossby number) are unstable. Remarkably, the growth rate of the unstable disturbance is a function of the spatial coordinates. At the same time, the corresponding boundary-value problem for normal modes has no smooth square-integrable solutions, which would normally be regarded as stability.

We conclude that (potentially) stable vortices can be found only among ageostrophic vortices. Since this assumption cannot be verified analytically due to complexity of the primitive equations, we verify it numerically for the particular case of two-layer stratification.

1. Introduction

One of the most puzzling features of oceanic rings and lenses is their longevity; they often persist for years (Lai & Richardson 1977; Olson 1991). The theoretical studies of Paldor & Nof (1989) and Ripa (1992), on the other hand, indicate that large-amplitude circular vortices are unstable (these results were obtained for a two-layer ocean with the lower layer at rest). In order to resolve the apparent contradiction between observation and theory, Dewar & Killworth (1995) considered two-layered vortices with a non-zero circulation in the lower layer and observed that unstable modes disappear for co-rotating vortices. Remarkably, the instability disappeared for very low values of the deep-flow velocity, so the vertical shear was, in fact, strong.

However, this result does not seem to be applicable to *geostrophic* vortices, i.e. vortices with small Rossby number, which are clearly unstable with respect to short-wave disturbances. Indeed, short waves may not be sensitive to the horizontal shear and therefore 'perceive' a vortex as a parallel quasi-geostrophic flow, and parallel quasi-geostrophic flows in a two-layer fluid on the *f*-plane are unstable (Phillips 1954). Thus, Dewar & Killworth's (1995) result resolves the old contradiction at the price of introducing a new one.

The main aim of the present paper is this new contradiction. It will be demonstrated that, although geostrophic‡ vortices with co-rotating deep flow may be stable with respect to harmonic normal modes, they are still unstable with respect to non-harmonic disturbances. This conclusion will be obtained for geostrophic vortices of arbitrary

† Present address: Department of Mathematics, University of Warwick, Coventry CV4 7AL, UK.

‡ Here and hereinafter, the term 'geostrophic' will exclude 'quasi-geostrophic', i.e. the displacement of isopycnal surfaces will always be assumed large.

shape and stratification. It will also be demonstrated that ageostrophic vortices can be stable even if their Rossby number is as low as 0.3.

In §2 we shall derive a relatively simple set of equations describing large-amplitude geostrophic flows on the f-plane, and in §§3–5 we shall use it to examine the stability of vortices. In §6, we shall examine numerically the stability of two-layer ageostrophic vortices.

2. Basic equations

Consider a flow of continuously stratified fluid bounded by two horizontal rigid planes, on the f-plane. The equations, governing the pressure p, velocity (u, v, w) and density ρ, are

$$u_t + uu_x + vu_y + wu_z + \frac{1}{\rho_0} p_x = fv, \tag{2.1a}$$

$$v_t + uv_x + vv_y + wv_z + \frac{1}{\rho_0} p_y = -fu, \tag{2.1b}$$

$$\frac{1}{\rho} p_z = -g, \tag{2.1c}$$

$$\rho_t + u\rho_x + v\rho_y + w\rho_z = 0, \tag{2.1d}$$

$$u_x + v_y + w_z = 0, \tag{2.1e}$$

where (x, y, z) and t are the spatial coordinates and time, f is the Coriolis parameter, g is the acceleration due to gravity and ρ_0 is the mean density of the fluid (the Boussinesq approximation implied). Instead of the continuity equation (2.1e), we shall derive the vorticity equation according to

$$(2.1b)_x - (2.1a)_y - (f + v_x - u_y) \times (2.1e).$$

Following routine calculations, we obtain

$$(v_x - u_y)_t + u(v_x - u_y)_x + v(v_x - u_y)_y + w(v_x - u_y)_z + w_z(v_x - u_y) + w_x v_z - w_y u_z = fw_z. \tag{2.2}$$

Equations (2.1a–d) and (2.2) should be supplemented by the no-flow condition at the rigid boundaries

$$w = 0 \quad \text{at} \quad z = -H_0, 0, \tag{2.3}$$

where H_0 is the total depth of the ocean.

In order to scale the governing equations, we shall assume that the displacement of isopycnal surfaces is comparable to the depth of the 'active' layer. With respect to the latter, we shall consider the general case, i.e. assume that it is comparable to the total depth of the ocean. Thus, the density anomaly $(\rho - \rho_0)$ will be scaled by the global density variation $\Delta\rho$, and z will be scaled by H_0. The hydrostatic approximation then implies that

$$P = g\,\Delta\rho\, H_0, \tag{2.4a}$$

where P is the pressure scale. We shall also assume that the flow is near geostrophic balance, i.e.

$$U = \frac{P}{f\rho_0 L}, \quad T = \frac{L}{U}, \tag{2.4b}$$

where U, T and L are the velocity, time and spatial scales, respectively. The scale W of the vertical velocity can be determined by comparing the advection terms and right-hand side in the vorticity equation (2.2):

$$W = \frac{H_0 U^2}{fL^2}. \tag{2.4c}$$

Now we can introduce the non-dimensional variables:

$$\left.\begin{aligned} t_* &= t/T, \\ x_* &= x/L, \qquad y_* = y/L, \quad z_* = z/H_0, \\ u_* &= u/U, \qquad V_* = v/U, \quad w_* = w/W, \\ p_* &= (p-\rho_0 gz)/P, \quad \rho_* = (\rho-\rho_0)/\Delta\rho. \end{aligned}\right\} \tag{2.5}$$

Substituting (2.4) and (2.5) in the governing equations (2.1*a–d*) and (2.2), (2.3), and omitting the asterisks, we have

$$\varepsilon(u_t + uu_x + vu_y) + \varepsilon^2 wu_z + p_x = v, \tag{2.6a}$$

$$\varepsilon(v_t + uv_x + vv_y) + \varepsilon^2 wv_z + p_y = -u, \tag{2.6b}$$

$$p_z = -\rho, \tag{2.6c}$$

$$\rho_t + u\rho_x + v\rho_y + \varepsilon w\rho_z = 0, \tag{2.6d}$$

$$\begin{aligned}(v_x-u_y)_t + u(v_x-u_y)_x + v(v_x-u_y)_y \\ + \varepsilon[w_z(v_x-u_y) + w(v_x-u_y)_z + w_x u_z - w_y u_z] = w_z.\end{aligned} \tag{2.7}$$

$$w = 0 \quad \text{at} \quad z = -1, 0, \tag{2.8}$$

where

$$\varepsilon = \frac{g\,\Delta\rho\, H_0}{fL^2} = \frac{U}{fL} \tag{2.9a}$$

is the Burger/Rossby number (for flows with large displacement of isopycnals, *Ro* and *Bu* always coincide). We shall assume that the flow is geostrophic, i.e.

$$\varepsilon \ll 1. \tag{2.9b}$$

Omitting terms proportional to ε in (2.6)–(2.8), we obtain

$$v = p_x, \quad u = -p_y, \quad \rho = -p_z, \tag{2.10}$$

$$\rho_t + u\rho_x + v\rho_y = 0, \tag{2.11}$$

$$(v_x-u_y)_t + u(v_x-u_y)_x + v(v_x-u_y)_y = w_z, \tag{2.12}$$

$$w = 0 \quad \text{at} \quad z = -1, 0. \tag{2.13}$$

Equations (2.10)–(2.13) are the desired asymptotic equations. They can be rewritten in a more convenient form, if (2.12) is integrated with respect to z over $(-1, 0)$. Taking into account the boundary conditions (2.13), one obtains

$$\int_{-1}^{0} [(v_x-u_y)_t + u(v_x-u_y)_x + v(v_x-u_y)_y]\,\mathrm{d}z = 0. \tag{2.14}$$

Finally, we substitute the geostrophic/hydrostatic conditions (2.10) into (2.11), (2.14) and obtain

$$p_{zt}+J(p,p_z)=0, \quad \int_{-1}^{0}[\nabla^2 p_t+J(p,\nabla^2 p)]\,\mathrm{d}z=0, \tag{2.15}$$

where $J(p,q)=p_x q_y-p_y q_x$. Equations similar to (2.15) were derived by Benilov (1993), Young (1994) and Ripa (1998). It is worth mentioning that, if the displacement of isopycnal surfaces is small, (2.15) coincides with the long-wave limit of the quasi-geostrophic equation.

3. Equations for linear disturbances

In this section, asymptotic equations (2.15) will be used for describing harmonic disturbances (normal modes) and, also, disturbances with arbitrary dependence on time.

Equation (2.15) admits the following steady solution describing a radially symmetric vortex:

$$p=P(r,z), \tag{3.1}$$

where $r=(x^2+y^2)^{1/2}$. We shall consider isolated vortices in an unbounded ocean, i.e.

$$P_x, P_y \to 0 \quad \text{as} \quad r\to\infty. \tag{3.2}$$

The stability of solution (3.1) will be examined within the framework of asymptotic equations (2.15).

First, we rewrite (2.15) in the cylindrical variables

$$\nabla^2 p=\frac{1}{r_2}p_{\phi\phi}+\frac{1}{r}(rp_r)_r, \quad J(p,q)=\frac{1}{r}(p_r q_\phi-p_\phi q_r),$$

where ϕ is the polar angle. We assume that the vortex is perturbed by a small disturbance:

$$p(t,r,\phi,z)=P(r,z)+p'(t,r,\phi,z). \tag{3.3}$$

Substituting (3.3) into (2.15) and omitting nonlinear terms, we obtain

$$\left.\begin{aligned} p'_{zt}+\frac{1}{r}P_r p'_{z\phi}-\frac{1}{r}p'_\phi P_{zr}=0,\\ \int_{-1}^{0}\left(\nabla^2 p'_t+\frac{1}{r}P_r\nabla^2 p'_\phi-\frac{1}{r}p'_\phi\nabla^2 P_r\right)\mathrm{d}z=0. \end{aligned}\right\} \tag{3.4}$$

First, we shall consider harmonic disturbances

$$p'(t,r,\phi,z)=q(r,z)\,\mathrm{e}^{\mathrm{i}\omega t-\mathrm{i}n\phi}, \tag{3.5}$$

where ω is the frequency, and n is the azimuthal wavenumber. Substitution of (3.5) into (3.4) yields

$$(\omega-n\Omega)\,q_z+n\Omega_z\,q=0, \tag{3.6a}$$

$$\int_{-1}^{0}\left\{(\omega-n\Omega)\left[(rq_r)_r-\frac{1}{r}n^2 q\right]-n\left[\frac{1}{r}(r^2\Omega)_r\right]_r q\right\}\mathrm{d}z=0, \tag{3.6b}$$

where

$$\Omega(r,z)=\frac{1}{r}P_r$$

is the angular velocity of the fluid. It follows from (3.2) that

$$\Omega\to 0 \quad \text{as} \quad r\to\infty. \tag{3.7}$$

Equation (3.6*a*) can be readily solved:

$$q(r,z)=[\omega-n\Omega(r,z)]\,\psi(r), \tag{3.8}$$

where the undetermined function $\psi(r)$ describes the horizontal structure of the disturbance.† Substitution of (3.8) into (3.6*b*) yields the following equation for $\psi(r)$:

$$(rS\psi_r)_r-\left(\frac{1}{r}n^2S+S_r\right)\psi=0, \tag{3.9}$$

where

$$S(r)=\int_{-1}^{0}[\omega-n\Omega(r,z)]^2\,\mathrm{d}z. \tag{3.10}$$

An equation similar to (3.9) has been derived for parallel flows by Tai & Niiler (1985) and Benilov (1993).

It is convenient to introduce the barotropic and baroclinic components of the vortex,

$$U(r)=\int_{-1}^{0}\Omega\,\mathrm{d}z, \quad V(r)=\left[\int_{-1}^{0}(\Omega-U)^2\,\mathrm{d}z\right]^{1/2},$$

respectively. In terms of U and V, (3.10) becomes

$$S(r)=(\omega-nU)^2+n^2V^2. \tag{3.11}$$

At the centre of the vortex ψ satisfies the standard condition

$$\psi=0 \quad \text{at} \quad r=0. \tag{3.12}$$

We shall also require that disturbances have finite kinetic energy:

$$K=\int_{-1}^{0}\int_{0}^{2\pi}\int_{0}^{\infty}\left\{|p_r'|^2+\frac{1}{r^2}|p_\phi'|^2\right\}r\,\mathrm{d}r\,\mathrm{d}\phi\,\mathrm{d}z<\infty.$$

Taking into account (3.5), (3.8) and (3.7), one can reduce this constraint to

$$\int_0^\infty|\psi_r|^2r\,\mathrm{d}r<\infty, \quad \int_0^\infty\frac{1}{r}|\psi|^2\,\mathrm{d}r<\infty. \tag{3.13}$$

Equations (3.9), and (3.11)–(3.13) form a boundary-value problem for normal modes described by ω and $\psi(r)$.

In addition to the harmonic disturbances (normal modes), we shall consider non-harmonic disturbances, i.e. replace (3.5) with

$$p'(t,r,\phi,z)=q(t,r,z)\,\mathrm{e}^{-\mathrm{i}n\phi}.$$

† In contrast to the exact primitive equations, the asymptotic set (2.15) always allows one to find the vertical structure of the disturbance explicitly.

Routine calculations, similar to the harmonic case, resolve the vertical structure of the solution:

$$q(t,r,z) = -\left[\mathrm{i}\frac{\partial}{\partial t} + n\Omega(r,z)\right]\psi(t,r)$$

(observe that the horizontal profile of the disturbance $\psi(t,r)$ now depends on time). Eventually, we obtain the following governing equation:

$$(r\hat{S}\psi r)_r - \left(\frac{1}{r}n^2\hat{S} + \hat{S}_r\right)\psi = 0, \tag{3.14}$$

where the operator $\hat{S}$ is given by

$$\hat{S} = \left(\mathrm{i}\frac{\partial}{\partial t} + nU\right)^2 + n^2V^2 \tag{3.15}$$

(recall that U and V are the barotropic and baroclinic components of the vortex, respectively). The conditions guaranteeing that the energy is finite are

$$\int_0^\infty |\psi_{rt}|^2 r\,\mathrm{d}r < \infty, \quad \int_0^\infty \frac{1}{r}|\psi_t|^2\,\mathrm{d}r < \infty. \tag{3.16}$$

Similar to the harmonic case, ψ should vanish at the centre of the vortex (i.e. satisfy condition (3.12)).

4. Evolution of linear disturbances

In this section, we shall compare the solution to the normal mode problem (3.9), (3.11)–(3.13) the solution to the initial-value problem (3.14)–(3.16), (3.12). Although we shall, in some instances, consider the case of arbitrary azimuthal wavenumber n, it turns out that many meaningful results can be extracted from the simplest particular case $n = 1$.

4.1. *Harmonic disturbances*

It is convenient to rewrite (3.9), (3.11)–(3.13) in terms of $\chi(r) = (1/r)\psi(r)$:

$$(r^3 S\chi_r)_r - (n^2-1)rS\chi = 0, \tag{4.1a}$$

$$S = (\omega - nU)^2 + n^2V^2, \tag{4.1b}$$

$$\int_0^\infty r^3|\chi_r|^2\,\mathrm{d}r < \infty, \quad \int_0^\infty r|\chi|^2\,\mathrm{d}r < \infty, \tag{4.1c}$$

$$\lim_{r\to 0}(r\chi) = 0. \tag{4.1d}$$

Observe that, if $n = 0$ (radially symmetric disturbance), equation (4.1a) is satisfied by

$$\omega = 0, \quad \chi = \text{arbitrary},$$

which corresponds to steady infinitesimal change of the vortex's form. Thus, we shall assume that $n \geqslant 1$.

It can be readily demonstrated (see Appendix A) that, for a vortex with non-zero baroclinic component ($V \not\equiv 0$), equations (4.1) have no stable solutions. This result,

however, does not prove instability, because (4.1) may have no unstable solutions either. For example, if $n = 1$ and $U(r)$ and $V(r)$ are continuous functions, the fundamental solution of (4.1*a*)

$$\chi = c_1 + c_2 \int \frac{\mathrm{d}r}{r^3 S}$$

does not satisfy conditions (4.1*c*, *d*) for any values of the constants $c_{1,2}$. Thus, it appears logical to conclude that geostrophic vortices are stable with respect to disturbances of the first azimuthal mode.

In the next subsection we shall demonstrate that the non-existence of unstable harmonic disturbances does not guarantee stability.

4.2. *Non-harmonic disturbances*

First, we rewrite (3.14)–(3.16), (3.12) in terms of $\chi(t, r) = (1/r)\,\psi(t, r)$:

$$(r^3 \hat{S}\chi_r)_r - (n^2 - 1)\,\hat{S}r\chi = 0, \tag{4.2a}$$

$$\hat{S} = \left(\mathrm{i}\frac{\partial}{\partial t} + nU\right)^2 + n^2 V^2, \tag{4.2b}$$

$$\int_0^\infty r^3 |\chi_{rt}|^2 \,\mathrm{d}r < \infty, \quad \int_0^\infty r |\chi_t|^2 \,\mathrm{d}r < \infty, \tag{4.2c}$$

$$\lim_{r \to 0} (r\chi) = 0. \tag{4.2d}$$

As before, we consider the simplest case $n = 1$, where (4.2*a*) can be reduced to

$$r^3[-\chi_{rtt} + 2\mathrm{i}U\chi_r + (U^2 + V^2)\,\chi_r] = \text{const}. \tag{4.3}$$

Equation (4.2*d*) implies that const = 0, and the solution to (4.3) becomes

$$\chi_r = A(r) \exp\{[\mathrm{i}U(r) + V(r)]\,t\} + B(r) \exp\{[\mathrm{i}U(r) - V(r)]\,t\}, \tag{4.4}$$

where $A(r)$ and $B(r)$ are determined by the initial conditions. Evidently, the first term in (4.4) grows exponentially (the baroclinic component $V(r)$ of the flow is assumed positive) which means instability. In contrast to harmonic disturbances, the growth rate

$$\mathrm{Im}\,\omega = V(r)$$

and azimuthal phase speed

$$\frac{\mathrm{Re}\,\omega}{n} = U(r)$$

of disturbance (4.4) depend on the spatial coordinate r!

We conclude that the non-existence of harmonic normal modes does not guarantee (at least, in this case) the non-existence of exponentially growing disturbances.

5. Discussion

(i) We have demonstrated that large-amplitude geostrophic vortices are unstable with respect to disturbances with $n = 1$. It should emphasized, however, that the first azimuthal mode is not necessarily the fastest growing. In fact, there is numerical evidence (see below) that the instability is dominated by short disturbances.

(ii) It is worth noting that the asymptotic equations (2.2) are also applicable to quasi-geostrophic (small-amplitude) motion with spatial scale much larger than the deformation radius. Accordingly, we conclude that large-scale quasi-geostrophic vortices are also unstable, which agrees with conclusions of Helfrich & Send (1988) and Flierl (1988).

(iii) Observe that, in principle, disturbance (4.4) can be made harmonic. Indeed, choosing a point $r = r_0$ such that $V(r_0) \neq 0$, we put

$$A(r) = \delta(r - r_0), \quad B(r) = 0,$$

where $\delta(r)$ is the Dirac delta-function. Equation (4.4) then becomes

$$\chi_r(r, t) = \delta(r - r_0) \exp\{[\mathrm{i}U(r_0) + V(r_0)]\, t\}. \tag{5.1}$$

This solution, however, has infinite energy and therefore does not satisfy conditions (4.1 *c*). Nevertheless, we can use (5.1) in rewriting solution (4.4) as a Fourier integral:

$$\chi_r = \int_0^\infty A(r_0)\, \delta(r - r_0) \exp\{[\mathrm{i}U(r_0) + V(r_0)]\, t\}\, \mathrm{d}r_0 + \int_0^\infty B(r_0)\, \delta(r - r_0) \exp\{[\mathrm{i}U(r_0) - V(r_0)]\, t\}\, \mathrm{d}r_0.$$

This equality shows that an arbitrary disturbance of the first azimuthal mode ($n = 1$) can be represented by a superposition of 'elemental' disturbances localized in infinitesimal 'rings' of radius r_0.

(iv) Equation (5.1) may also be interpreted as an eigenfunction of the continuous spectrum similar to that of Rayleigh's equation (describing plane Poiseuille flow, e.g. Dikiy 1976). Both have δ-function irregularities and both correspond to critical levels. The only difference is that, in the problem at hand, the critical levels occur at complex values of the phase velocity and therefore cause instability.

(v) It should be mentioned that disturbances like (4.4), with growth rates depending on spatial coordinates, are by no means new: similar solutions have been examined by Orr (1907) and Boyd (1983) for unbounded Couette flow, by Farrel (1982, 1984, 1985, 1989) for baroclinic flows, by Farrel (1987) for barotropic flows, and by Farrel (1988), Gustavsson (1991) and Butler & Farrel (1992) for Poiseuille flow. It was demonstrated that there exists a large class of non-modal disturbances that can grow to finite amplitudes within the framework of linearized equations. Although these disturbances eventually decay, the transient amplification can be very vigorous (by a factor of 1000) and can 'destroy' the flow through nonlinear effects (neglected by the linearized theory).

The difference between the 'transient' disturbances considered in the above-mentioned papers and solution (4.4) is that the latter keeps growing at $t \to \infty$ and never decays.

It is interesting to speculate on what is the equivalent of (4.4) and (5.1) within the framework of the exact primitive equations. There seems to be three possibilities:

(*a*) Equation (5.1) may correspond to a 'normal' (square-integrable) unstable eigenmode with spatial scale much smaller than the radius of the vortex (similar examples for parallel flows were examined by Killworth 1980).

(*b*) The linearized primitive equations may admit a non-modal solution similar to (4.4) (i.e. one that exponentially grows at $t \to \infty$ and never decays).

(*c*) Equation (4.4) may correspond to a 'transient' solution (i.e. one that grows for a long time, but eventually decays).

Possibility (*a*) implies that Dewar & Killworth (1995) missed some of the eigenfunctions of the linearized primitive equations, which seems unlikely. Possibility (*b*) seems unlikely because the primitive equations describe free gravity waves, which would not stay on the infinitesimal 'ring' corresponding to the δ-function irregularity. Thus, possibility (*c*) seems to be the only probable one. We note that, whichever possibility is true, all geostrophic vortices are unstable anyway (with respect to either modal or non-modal disturbances).

6. Ageostrophic vortices in a two-layer fluid

In § 5 we have demonstrated that all geostrophic vortices are unstable. The inevitable conclusion to be drawn is that stable vortices, if any, must be ageostrophic or, equivalently, must be of radius comparable to the deformation radius (see constraint (2.9)). In this case, however, we cannot use our asymptotic equations (2.15), and no analytic results were obtained for ageostrophic vortices. Instead, we examined them numerically for the (simplest) case of two-layer stratification. Since the normal-mode analysis cannot be relied upon in our case (as demonstrated in § 4), we simulated the evolution of vortices using the primitive equations. Apart from modelling ageostrophic vortices, we tried to verify the analytic solution (4.4) for geostrophic vortices – which, however, turned out to be impossible (see § 5, point (iv)).

We used the following non-dimensional variables:

$$\begin{aligned} t_* &= tf, \\ x_* &= x/R_d, \qquad y_* = y/R_d, \\ u_{j*} &= u_j/(fR_d), \quad v_{j*} = v_j/(fR_d), \\ p_{j*} &= p/(g'H_0), \quad h_{j*} = h_j/H_0, \end{aligned}$$

where the subscript $j = 1, 2$ is the layer number (1 = upper), $g' = g\Delta\rho/\rho_0$ is the reduced acceleration due to gravity, and $R_d = (g'H_0)^{1/2}/f$ is the deformation radius based on the total depth of the ocean. For all physical estimates, we shall assume that

$$H_0 = 4 \text{ km}, \quad f = 6.25 \text{ days}^{-1}, \quad R_d = 60 \text{ km}, \tag{6.1}$$

which are typical for the open ocean at mid latitudes (say, 30°).

In terms of the non-dimensional variables, the two-layer primitive equations are (asterisks omitted)

$$\left.\begin{aligned} \left(\frac{\partial}{\partial t} + u_j\frac{\partial}{\partial x} + v_j\frac{\partial}{\partial y}\right)u_j + \frac{\partial p_j}{\partial x} &= v_j, \\ \left(\frac{\partial}{\partial t} + u_j\frac{\partial}{\partial x} + v_j\frac{\partial}{\partial y}\right)v_j + \frac{\partial p_j}{\partial y} &= -u_j, \\ \frac{\partial h_j}{\partial t} + \frac{\partial}{\partial x}(h_j u_j) + \frac{\partial}{\partial y}(h_j v_j) &= 0, \\ h_1 + h_2 = 1, \quad p_1 - p_2 &= h_1. \end{aligned}\right\} \tag{6.2}$$

The initial conditions for the vortex are discussed in Appendix B, § B.1. Roughly speaking, a steady vortex is determined by three main parameters: the effective radius

Run no.	r_0	A_1	A_2	α	
1	5	0.17	0	0.027	Unstable
2	5	−0.17	0	0.023	Unstable
3	5	0.187	0.017	0.029	Unstable
4	5	−0.017	−0.017	0.024	Unstable
5	2.5	0.17	0	0.028	Unstable
6	2.5	−0.17	0	0.020	Unstable
7	1.5	0.17	0	0.034	Stable
8	1.5	−0.17	0	0.020	Unstable
9	1	−0.17	0	0.017	Unstable
10	0.5	−0.17	0	0.012	Unstable

TABLE 1. Parameters of the two-layer vortices simulated using primitive equations: r_0 is the non-dimensional radius of the vortex (scaled by the deformation radius R_d based on the total depth of the ocean); $A_{1,2}$ are the non-dimensional amplitudes of the pressure anomalies; α is the non-dimensional amplitude of the disturbance.

r_0 and the amplitudes $A_{1,2}$ of the pressure anomalies in the layers (the amplitude of the displacement of the interface is given by $\Delta h_1 = A_1 - A_2$). The 'background' ocean is characterized by a single parameter, the mean depth h_{1b} of the upper layer.

The initial condition for the disturbance superposed on the vortex is discussed in Appendix B, §B.2. Generally, it was 10 times weaker than the flow of the vortex.

Equations (6.2) were simulated using the pseudospectral method with Fourier series and a tenth-order high-wavenumber filter. The time derivatives were evaluated using the fourth-order Runge–Kutta scheme. In order to control the accuracy, we monitored conservation of the extreme values of potential vorticity in each layer and the net energy and mass. The simulations were run for 123.2 days, or as long as the error in potential vorticity stayed under 5%. The errors in conservation of net energy and mass were always below 0.1%. In most cases, the resolution of 512×512 gridpoints had to be used, but for smaller vortices, it was sufficient to use 256×256 gridpoints.

6.1. *Results*

Ten initial-value simulations of vortices of various radii and amplitudes were performed on a Cray J90 – see table 1. The physical characteristics of the vortices (calculated using the values of H_0, f and R_d determined by (6.1)) are given in table 2. In all our simulations, we used the following non-dimensional values of the mean depth of the upper layer and the amplitude of the interfacial displacement:

$$h_{1b} = 0.25, \quad \Delta h_1 = \pm 0.17.$$

This means that the upper layer was four times thinner than the total depth of the ocean, and the displacement of the interface was 68% of the depth of the active layer. Given (6.1), this corresponds to

$$h_{1b^*} = 1 \text{ km}, \quad \Delta h_{1^*} = \pm 680 \text{ m}.$$

(Δh_{1^*} seems too large, but that is what we had to assume to obtain the 'correct' (typical) values of the swirl velocity of oceanic rings.) Runs 5–8 were intended to model moderate to strong (but not the strongest) oceanic rings, whereas runs 1–4 and 9–10 are included to illustrate how an increase or decrease in the vortex's radius affects its stability.

Run no.	Core	Ro_{max}	r_{0*} (km)	r_{u*} (km)	u_{max*} (m s^{-1})	T_{turn} (days)	
1	Cold	0.028	300	175	0.20	63	Unstable
2	Warm	0.026	300	175	0.20	63	Unstable
3	Cold	0.031	300	175	0.23	56	Unstable
4	Warm	0.028	300	175	0.22	58	Unstable
5	Cold	0.119	150	86	0.43	14	Unstable
6	Warm	0.096	150	88	0.38	17	Unstable
7	Cold	0.438	90	48	0.89	4	Stable
8	Warm	0.247	90	54	0.58	7	Unstable
9	Warm	0.480	60	38	0.78	3	Unstable
10	Warm	1.327	30	19	1.10	1	Unstable

TABLE 2. Physical parameters of the two-layer vortices simulated using primitive equations: *Ro* is the Rossby number based on the maximum velocity shear at $t = 0$; r_{0*} is the radius where the interfacial displacement decays by the factor 10; r_{u*} is the radius of maximum velocity; u_{max*} is the maximum velocity; T_{turn} is the turnaround time.

Figure 1 shows the evolution of warm- and cold-core vortices with $r_0 = 5$ and confirms our analytic result that geostrophic vortices are unstable.

The vortices shown in figure 2 are of the same vertical shear as those in figure 1, but have a weak co-rotating circulation in the lower layer. The fact that the co-rotating and non-co-rotating vortices are unstable approximately to the same extent suggests that co-rotation in the lower layer does not inhibit instability (see more on this below).

Figure 3 shows the evolution of warm- and cold-core vortices with $r_0 = 2.5$, which, however, can still be treated as geostrophic ($Ro \approx 0.1$, see table 2). Observe that the instability does not reduce the vortices to 'rubble' (which it did in the previous two cases), but just breaks them up into several, apparently stable, smaller eddies.

Figure 4 shows the evolution of warm- and cold-core vortices with $r_0 = 1.5$. The warm-core vortex is evidently stable, whereas the cold-core vortex is still unstable. We emphasize that this behaviour does not contradict our analytical conclusions, which predict that some (but not necessarily all ageostrophic vortices may be stable. Moreover, the two separate eddies 'produced' by the instability of the warm-core vortex eventually merge and form a stable vortex of about the same radius as the original one, although apparently of a different profile.

In order to pinpoint the stability threshold, we performed simulations for warm-core vortices with radii in between $r_0 = 1.5$ and $r_0 = 2.5$. The results suggest that the stability occurs for vortices with $r_0 \sim 2$, i.e. $Ro \sim 0.3$.

We also ran several simulations for smaller cold-core vortices (their warm-core counterparts do not exist due to the limitation imposed by the cyclostrophic condition – (see Appendix B, §B.1). The evolution of the vortex with $r_0 = 1$ was very similar to that of the cold-core vortex with $r_0 = 1.5$, but the vortex with $r_0 = 0.5$ behaved somewhat differently. The two smaller eddies which split from it – in contrast to the previous two cases – did not merge, but stabilized and steadily rotated around each other (see figure 5*a*).

Finally, in order to emphasize the importance of high accuracy in the simulation of vortex instability, we performed a lower-resolution (128×128 gridpoints) simulation of the warm-core vortex with $r_0 = 0.5$. Although the computational error in this run was relatively low (9.9%), it looks both quantitatively and qualitatively different from the higher-resolution (256×256 gridpoints) run – compare figures 5(*a*) and 5(*b*). Apart from the wrong positions of the eddies which split from the original vortex, the lower-accuracy simulation shows that these eddies eventually merge!

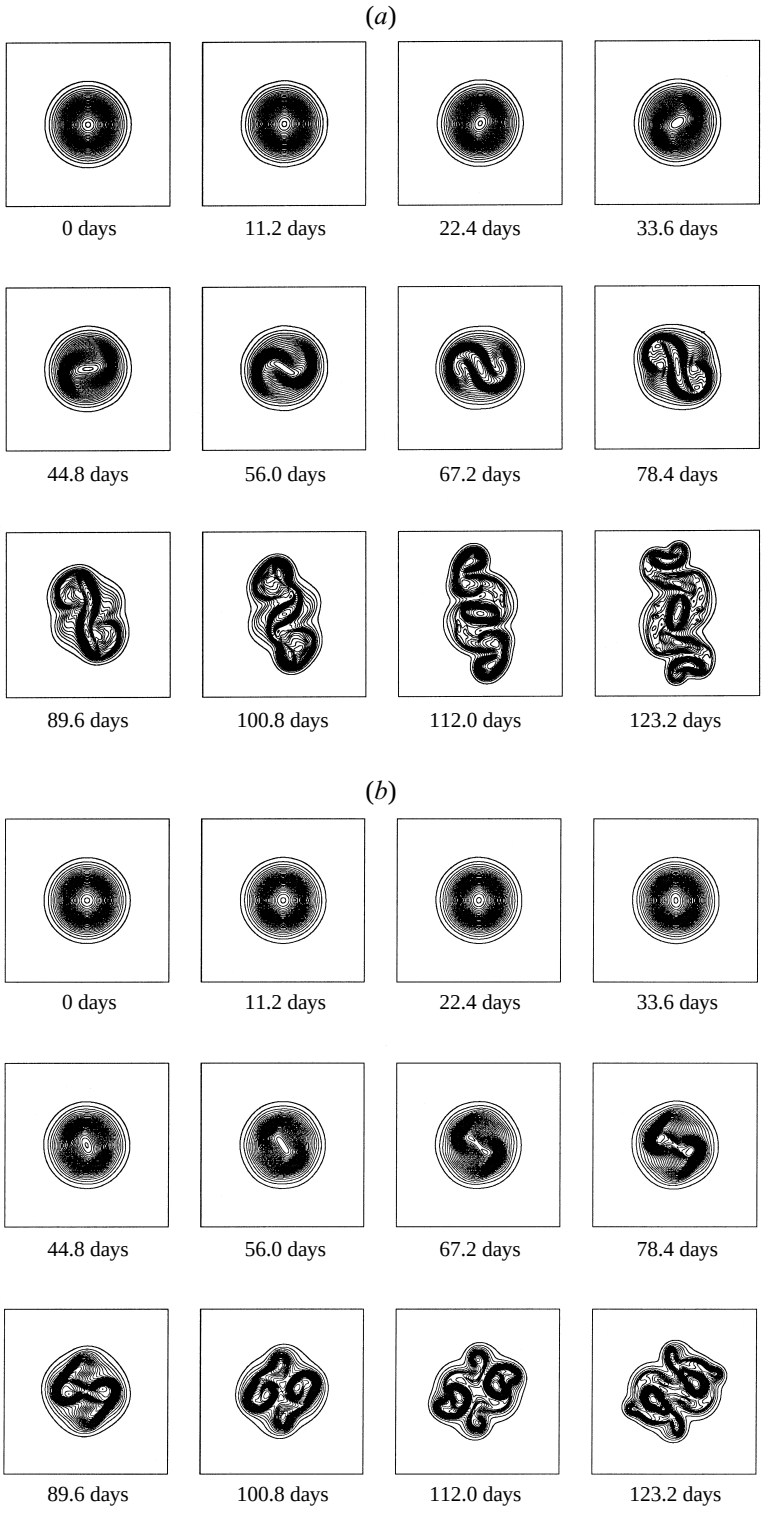

FIGURE 1. Evolution of the vortices with $r_0 = 5$ (for dimensional parameters see table 2, runs 1 and 2): (*a*) warm-core vortex, (*b*) cold-core vortex.

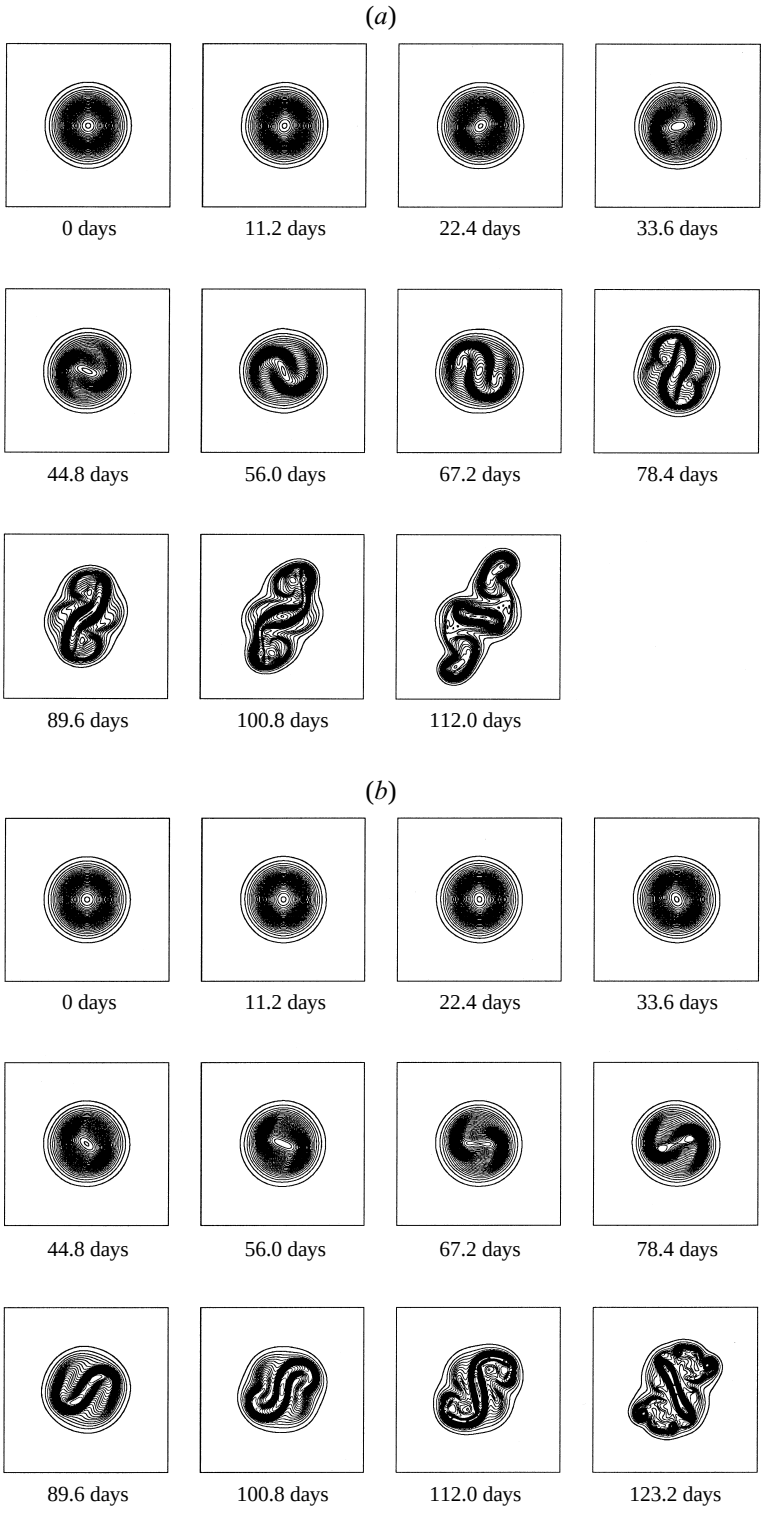

FIGURE 2. Evolution of the vortices with $r_0 = 5$ and co-rotation in the lower layer (for dimensional parameters see table 2, runs 3 and 4): (*a*) warm-core vortex, (*b*) cold-core vortex.

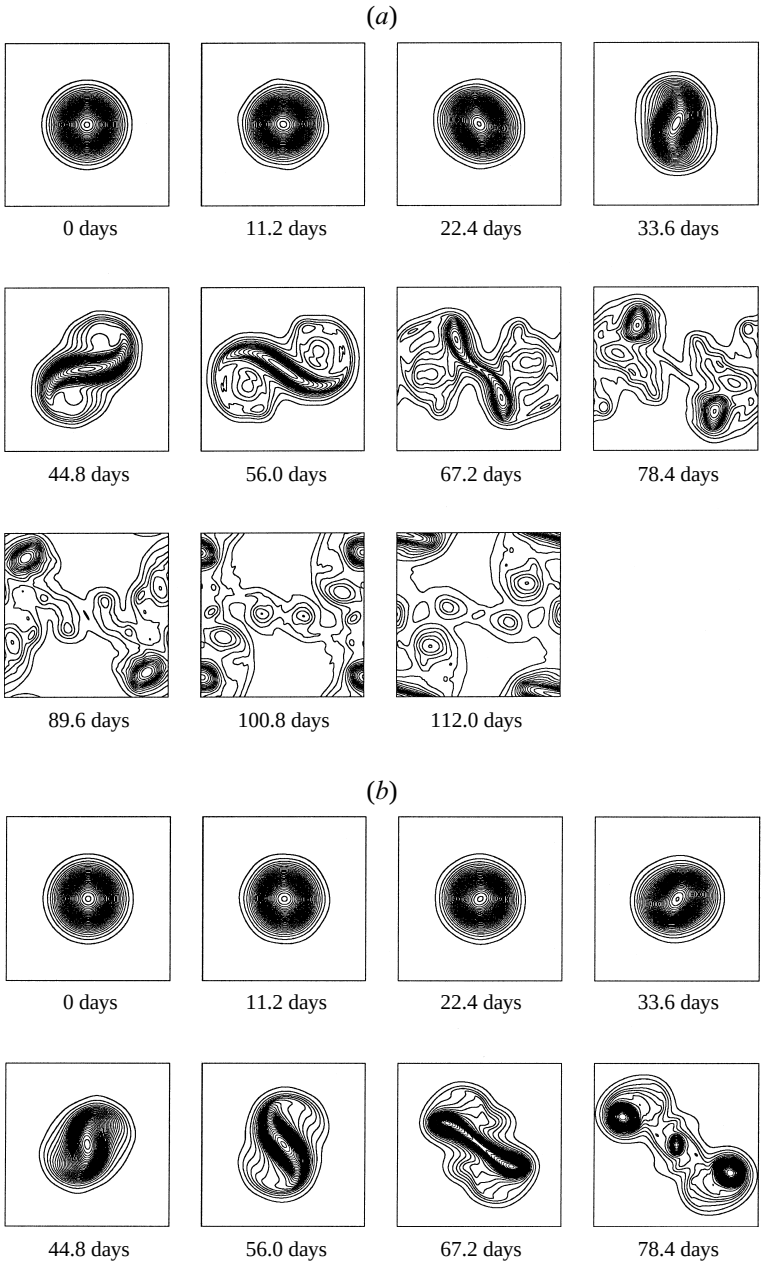

FIGURE 3. Evolution of the vortices with $r_0 = 2.5$ (for dimensional parameters see table 2, runs 5 and 6): (*a*) warm-core vortex, (*b*) cold-core vortex.

6.2. *Discussion*

In addition to the above figures (which provide a good qualitative description of the instability), we also 'measured' the following quantitative characteristic:

$$\mu(t) = \frac{\text{net kinetic energy of the upper layer}}{\text{total net kinetic energy}}. \tag{6.4}$$

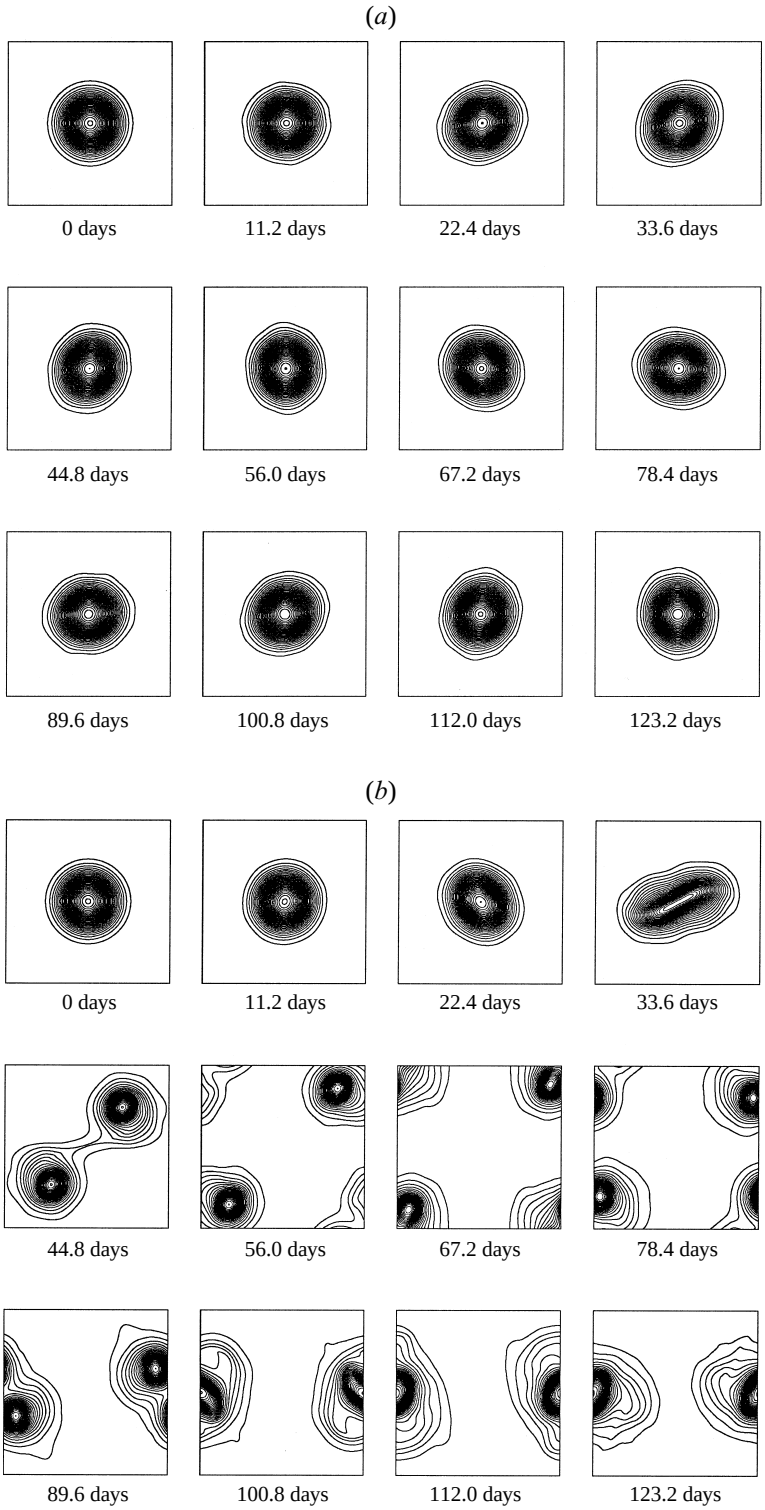

FIGURE 4. Evolution of the vortices with $r_0 = 1.5$ (for dimensional parameters see table 2, runs 7 and 8): (*a*) warm-core vortex, (*b*) cold-core vortex.

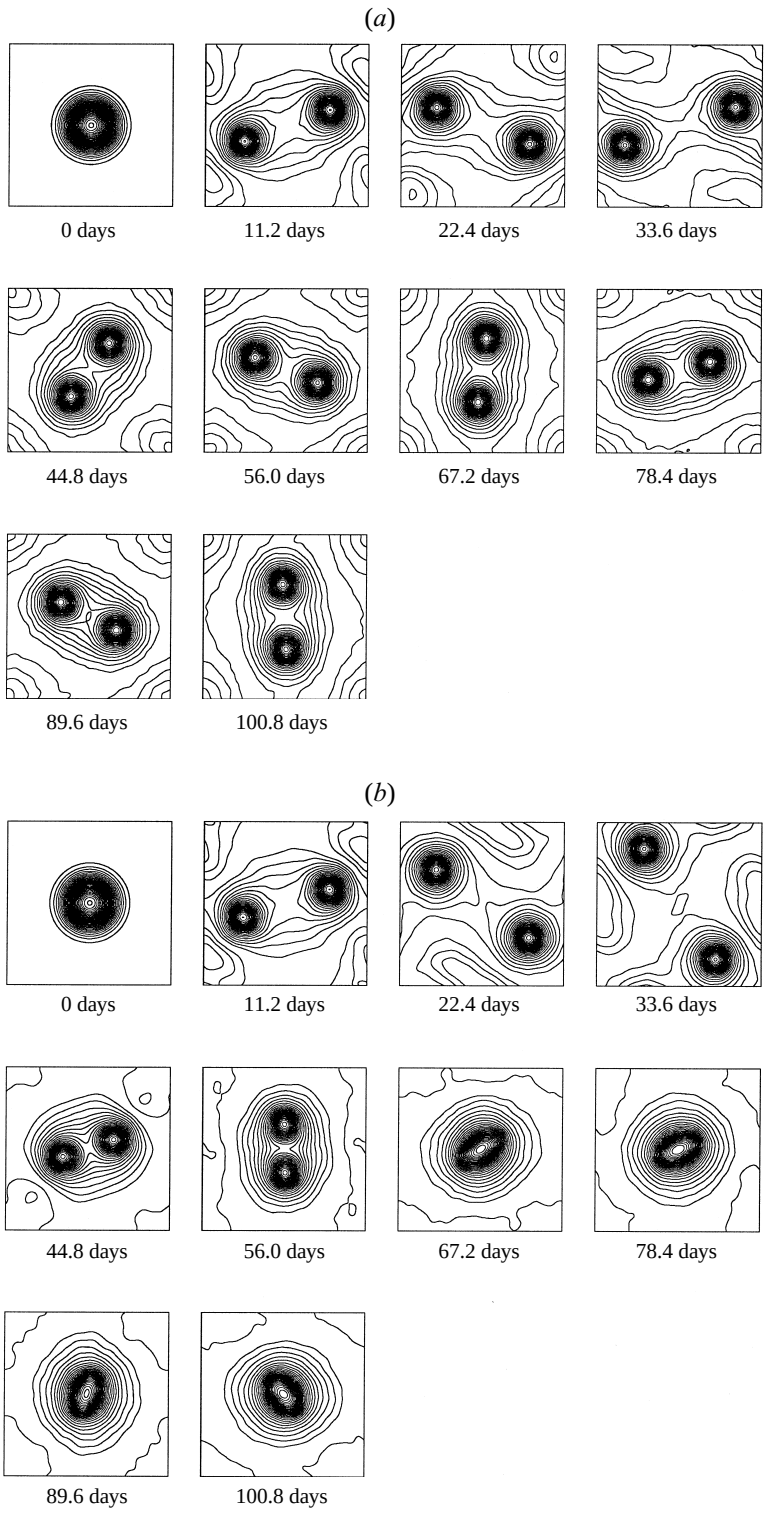

FIGURE 5. Evolution of the cold-core vortex with $r_0 = 0.5$ (for dimensional parameters see table 2, run 10): (*a*) high-resolution run, (*b*) low-resolution run.

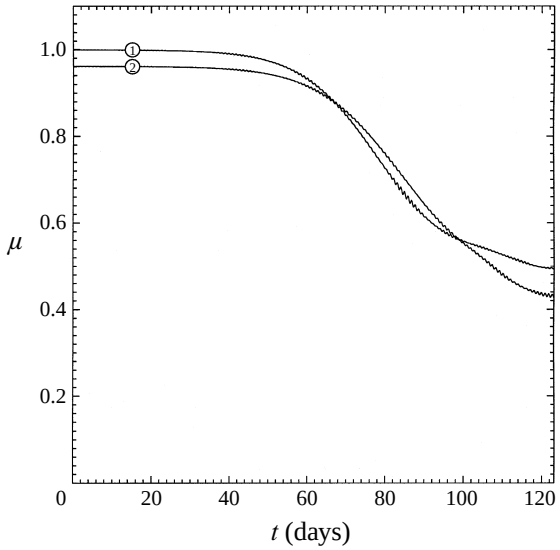

FIGURE 6. Comparison of vortices with co-rotation in the lower layer (curve 1), and vortices without co-rotation in the lower layer (curve 2). For the definition of μ, see (6.4). For dimensional parameters of the vortices, see table 2, runs 2 and 4.

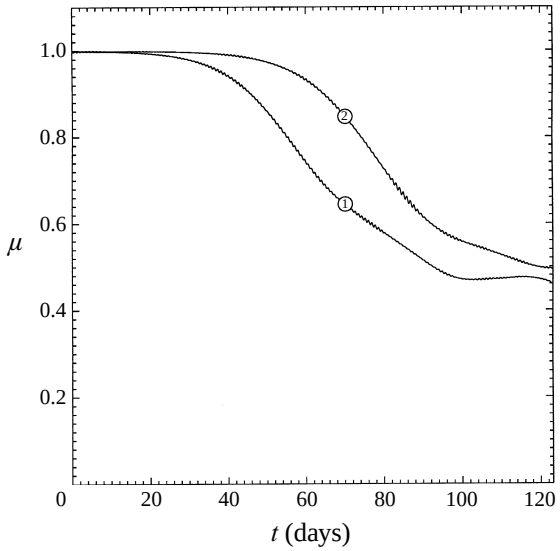

FIGURE 7. Comparison of warm-core vortices (curve 1), and cold-core vortices (curve 2). For dimensional parameters of the vortices, see table 2, runs 1 and 2.

This parameter will be used as an indicator of instability: if it changes, the instability is clearly taking place.

(i) μ was used to illustrate our conclusion that co-rotation in the lower layer does not inhibit instability. Figure 6 shows that the unstable disturbances on the co-rotating vortex develop slower than those on the non-co-rotating vortex only at the initial stage of instability (which agrees with the predictions of the linear theory of Dewar & Killworth 1995). When the disturbances grow to a certain amplitude, the instability of the co-rotating vortex catches up with that of the non-co-rotating vortex, and even

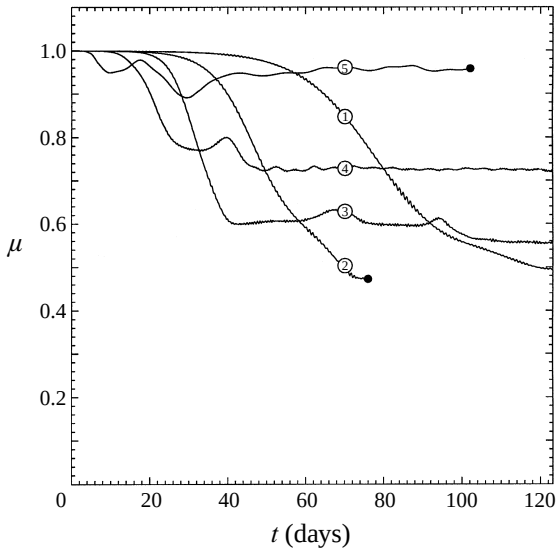

FIGURE 8. Comparison of cold-core vortices of different radii: $r_0 = 5$ (curve 1), $r_0 = 2.5$ (curve 2), $r_0 = 1.5$ (curve 3), $r_0 = 1$ (curve 4), $r_0 = 0.55$ (curve 5). For dimensional parameters of the vortices, see table 2, runs 2, 6 and 8–10. The black circle indicates that the corresponding simulation exceeded the accuracy threshold (5%).

becomes stronger. In any case, one way or the other, the difference between the two vortices is very slight.

(ii) It is interesting to compare the growth rates of instabilities of warm- and cold-core vortices (of the same radii and amplitudes). It turns out that, in all cases where both vortices were unstable, the cold-core vortex was marginally more unstable than its counterpart – see figure 7.

(iii) It is also interesting to compare the growth rates of instabilities of vortices of the same 'sign' but different r_0. The evolution of μ for cold-core vortices with $r_0 = 0.5$–5 is shown in figure 8. The features worth observing are:

(*a*) one can clearly see that the case where the instability reduces the original vortex to a turbulent patch is the odd one out – in all other cases the vortex breaks up into several smaller stable eddies (compare graph 1 with graphs 2–5);

(*b*) the instability of the smallest vortex $r_0 = 0.5$ takes place almost exclusively in the upper layer;

(*c*) the shorter the vortex, the faster the instability.

It should be emphasized, however, that the last conclusion holds only if the time is measured in the absolute terms. If we redraw each graph in figure 8 for t scaled by the turnaround time of the corresponding vortex (see table 2), this conclusion will change to the opposite: smaller vortices require a lot more turnarounds to break apart.

(iv) Figure 9 shows the evolution of the Rossby number defined as

$$Ro(t) = \max\left[\frac{\partial u(x, y, t)}{\partial y}\right]$$

for the warm- and cold-core vortices with $r_0 = 5$. Observe that in both cases the Rossby number grows with time. This indicates that the instability of geostrophic vortices takes place at wavelengths that are shorter than the radius of the vortex. There are three different aspects to this important conclusion.

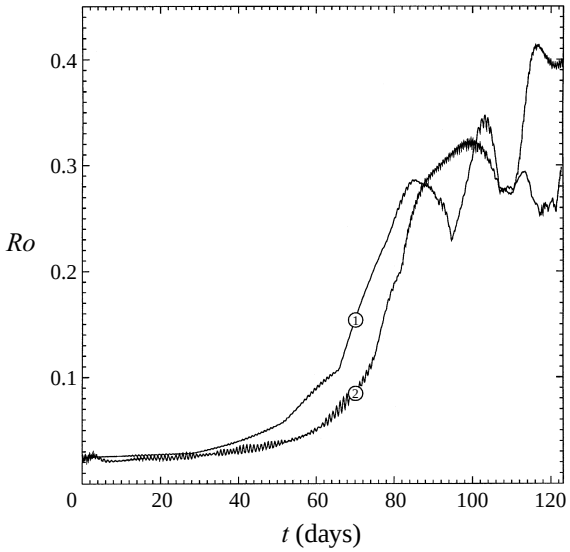

FIGURE 9. Evolution of the Rossby number of the vortices with $r_0 = 5$ for warm-core vortices (curve 1) and cold-core vortices (curve 2). For dimensional parameters of the vortices, see table 2, runs 1 and 2.

(*a*) First, it is in apparent contradiction with (4.4), which predicts instability on the scale of the vortex. In order to resolve the discrepancy, we note that (4.4) is just a particular solution with $n = 1$. Clearly, short disturbances (with $n \gg 1$) can also be unstable, which, in fact, agrees with a similar result for parallel flows (where the spatial scale of instability is comparable to the deformation radius – see Benilov & Reznik 1996).

(*b*) It should also be noted that the generation of short disturbances violates the applicability condition (2.9) of the asymptotic system (2.15) used in the analytical part of this paper. Thus, (2.15) only allows us to establish the fact of instability (with respect to long, geostrophic disturbances), but provides no means of investigating the long-term evolution of the unstable vortices (which is dominated by short waves). The latter task requires use of the primitive equations.

(*c*) Finally, the short-wave character of the instability explains why we have been unable to observe the analytic solution (4.4) in numerical simulations of geostrophic two-layer vortices. Given that short waves grow faster than the smooth component of the disturbance (described by (4.4)), the latter is virtually invisible in the solution. No matter how we filtered the initial condition, the numerical error always contaminated the simulation with short disturbances. We also tried to filter those continuously (which, in fact produced a reasonable agreement with the analytical solution), but this filtering also affected the accuracy, which made the results untrustworthy.

7. Conclusions

(i) Physically, our main result is the demonstration of instability of all geostrophic large-amplitude vortices on the *f*-plane regardless of their profile or stratification. We conclude that, theoretically, an oceanic ring may be stable only if it is ageostrophic (i.e. if its effective radius is of the order of the deformation radius). The stabilization occurs for vortices with Rossby number of the order of 0.3. For comparison, Olson (1991) reported rings with *Ro* as large as 0.77.

(ii) Our second conclusion is a methodological one: normal-mode analysis may not be representative, in some cases, of the stability properties of vortices. We have demonstrated that the normal-mode boundary-value problem, describing harmonic disturbances on a geostrophic vortex, has no smooth finite-energy solutions (stable or unstable). At the same time, the initial-value problem for non-harmonic disturbances does have an exponentially growing solution (the growth rate depending on the spatial variables). It is possible, however, to reduce such a solution to a harmonic disturbance, but the latter will have a δ-function singularity.

Finally, we should make it clear that conclusion (ii) was obtained using an asymptotic set of equations, which describes geostrophic disturbances on a geostrophic vortex (i.e. the wavelength of the former and the radius of the latter were assumed to be large in comparison with the deformation radius). It is not clear if the non-harmonic disturbances exist within the framework of the exact primitive equations.

This work was supported by Large Grant No. A39530698 of the Australian Research Council. We are grateful to Referee A for two valuable remarks and to Referee B, who drew our attention to transient modes.

Appendix A. Non-existence of stable solutions to equations (4.1) with $V(r) \neq 0$

We multiply (4.1 *a*) by the complex conjugate of χ and integrate by parts with respect to r over $(0, \infty)$. Using (4.1 *b*, *c*) and substituting (2.22), we obtain

$$\int_0^\infty [(nU-\omega)^2 + n^2 V^2][r^3 |\chi_r|^2 + (n^2-1) r |\chi|^2] \, \mathrm{d}r = 0. \tag{A 1}$$

Clearly, ω may not be real for $n \geqslant 1$.

Observe that this conclusion implies that

$$V(r) \neq 0.$$

Indeed, let us assume that there exists a point $r = r_0$ such that the baroclinic component of the flow vanishes: $V(r_0) = 0$. It can be readily demonstrated that, if

$$\omega = nU(r_0),$$

the eigenfunction may be singular

$$\chi = \frac{\text{const}}{r - r_0} + O(1),$$

and the integral in (A 1) diverges, which makes it invalid.

Appendix B. Initial conditions for numerical simulation of two-layer vortices

It is convenient to split the initial condition into two parts corresponding to the vortex and disturbance:

$$u_j = \bar{u}_j + u_j', \quad v_j = \bar{v}_j + v_j', \quad h_j = \bar{h}_j + h_j' \quad \text{at} \quad t = 0, \tag{B 1}$$

where the bars/primes correspond to the vortex/disturbance.

B.1. *Vortex*

The most common type of vortex considered in the literature is the Gaussian vortex:

$$\bar{h}_1 = h_{1b} + \Delta h_1 \exp(-\gamma r^2), \tag{B 2}$$

where h_{1b} is the unperturbed depth of the upper layer, Δh_1 is the amplitude of the interfacial displacement, and γ characterizes the radius of the vortex. We shall define the radius r_0 as the distance over which the amplitude of the vortex drops by the factor 10:

$$\gamma r_0^2 = \ln 10,$$

after which (B 2) becomes

$$\bar{h}_1 = h_{1b} + \Delta h_1 \exp\left[-(\ln 10)\left(\frac{r}{r_0}\right)^2\right]. \tag{B 3}$$

It turns out, however, that the Gaussian profile limits severely the amplitude of possible warm-core eddies. In order to illustrate this, we shall first consider the simplest case of vortices localized in the upper layer:

$$p_2 = 0.$$

The swirl velocity $s_1(r)$ in the upper layer satisfies the cyclostrophic relation

$$\frac{\mathrm{d}h_1}{\mathrm{d}r} = s_1 + \frac{1}{r}s_1^2,$$

and, in order to guarantee that s is real for all r, $\mathrm{d}h_1/\mathrm{d}r$ must satisfy

$$r + 4\frac{\mathrm{d}h_1}{\mathrm{d}r} > 0 \quad \text{for all} \quad r. \tag{B 4}$$

This condition severely restricts the allowable amplitude of vortex (B 3):

$$\Delta h_1 < \frac{r_0^2}{8 \ln 10}.$$

Assuming that $r_0 = 1$ (given (6.1), this amounts to $r_{0^*} = 60$ km, where r_{0^*} is the dimensional radius of the vortex), the maximum amplitude of a moderate-size warm-core Gaussian eddy localized in the upper layer, in an ocean 4 km deep, is just 217 m.

In order to model large-amplitude vortices, we used the following profile:

$$\bar{p}_j = \frac{A_j}{1 + 1.23(r/r_0)^4} \exp\left[-1.50\left(\frac{r}{r_0}\right)^2\right], \tag{B 5}$$

where $A_j\,(j = 1, 2)$ are the amplitudes of the pressure anomalies in the layers. The depth of the interface is given by

$$\bar{h}_1 = h_{1b} + \frac{\Delta h_1}{1 + 1.23(r/r_0)^4} \exp\left[-1.50\left(\frac{r}{r_0}\right)^2\right], \tag{B 6}$$

where $\Delta h_1 = A_1 - A_2$. The swirl velocities $\bar{s}_1$ and $\bar{s}_2$ are assumed to satisfy the condition of cyclostrophic balance:

$$\frac{\mathrm{d}\bar{p}_j}{\mathrm{d}r} = \bar{s}_j + \frac{1}{r}\bar{s}_j^2. \tag{B 7a}$$

Then, the components of the Cartesian velocities are determined by

$$\bar{u}_j = -\bar{s}_j \sin\phi, \quad \bar{v}_j = \bar{s}_j \cos\phi. \tag{B 7b}$$

Formulae (B 5)–(B 7) determine the initial condition for the vortex.

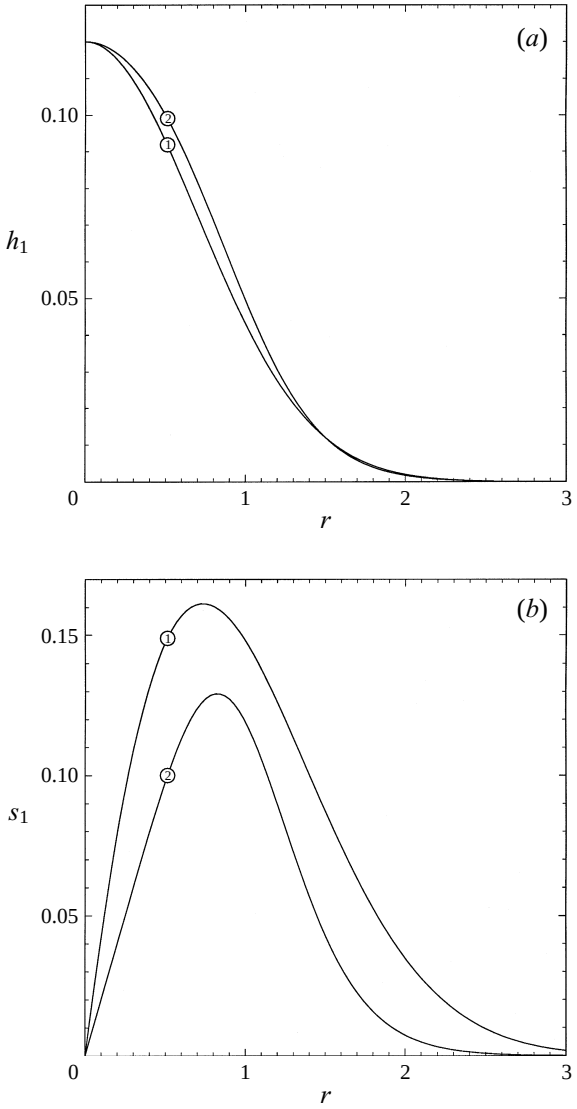

FIGURE 10. Comparison of the Gaussian vortex with vortex (B 6), (B 7): (*a*) displacement of the interface, (*b*) swirl velocity in the upper layer.

In order to compare the Gaussian vortex with the vortex given by (B 6), (B 7), we assume that the latter has no flow in the lower layer and plot the interfacial displacement and swirl velocity of the two vortices for

$$r_0 = 1.5, \quad A_1 = 0.12, \quad A_2 = 0$$

(see figure 10). One can see that the profiles of the interfacial displacements of the two vortices are fairly similar – see figure 10(*a*). The swirl velocity profiles, in turn, are different: the inner slope of vortex (B 6), (B 7) is less steep (see figure 10*b*), which allows it to reach a bigger amplitude before the velocity field becomes complex. For example, the limiting amplitude of warm-core vortex (B 6), (B 7) of radius 60 km and no flow in the lower layer, in an ocean 4 km deep, is 336 m (recall that the corresponding value for the Gaussian vortex is only 217 m).

B.2. *Disturbance*

Observe that allowable initial conditions for equations (6.2) must satisfy

$$\frac{\partial}{\partial x}(u_1 h_1 + u_2 h_2) + \frac{\partial}{\partial y}(v_1 h + v_2 h_2) = 0, \tag{B 8}$$

which follows from (6.2) (physically, (B 8) is a result of incompressibility of the fluid and its boundedness by horizontal rigid planes). The simplest way to ensure the validity of (B 8) is to introduce the barotropic streamfunction Ψ:

$$u_1 h_1 + u_2 h_2 = -\frac{\partial \Psi}{\partial y}, \quad v_1 h_1 + v_2 h_2 = \frac{\partial \Psi}{\partial x}. \tag{B 9}$$

As before, it is convenient to split the initial condition for Ψ into the vortex and disturbance parts:

$$\Psi_j = \bar{\Psi}_j + \Psi_j' \quad \text{at} \quad t = 0. \tag{B 10}$$

Substituting (B 1) and (B 10) into (B 9), and taking into account that

$$\bar{u}_1 \bar{h}_1 + \bar{u}_2 \bar{h}_2 = -\frac{\partial \bar{\Psi}}{\partial y}, \quad \bar{v}_1 \bar{h}_1 + \bar{v}_2 \bar{h}_2 = \frac{\partial \bar{\Psi}}{\partial x},$$

we obtain

$$\left.\begin{aligned} u_1' \bar{h}_1 + \bar{u}_1 h_1' + u_2' \bar{h}_2 + \bar{u}_2 h_2' &= -\frac{\partial \Psi'}{\partial y}, \\ v_1' \bar{h}_1 + \bar{v}_1 h_1' + v_2' \bar{h}_2 + \bar{v}_2 h_2' &= \frac{\partial \Psi'}{\partial x}. \end{aligned}\right\} \tag{B 11}$$

We assume, for simplicity, that the interface and the lower-layer flow are not initially perturbed:

$$h_1' = 0, \quad u_2' = 0, \quad v_2' = 0. \tag{B 12}$$

(It can be demonstrated that at $t > 0$ the disturbance immediately penetrates the lower layer.) Thus, (B 11) yields

$$u_1' = -\frac{1}{\bar{h}_1}\frac{\partial \Psi'}{\partial y}, \quad v_1' = \frac{1}{\bar{h}_1}\frac{\partial \Psi'}{\partial x}. \tag{B 13a}$$

We used the following expression for Ψ':

$$\Psi' = \alpha(\bar{h}_1 - h_{1b})\,\bar{h}_1 \left(\cos\frac{2\pi x}{r_0} - \cos\frac{2\pi y}{r_0}\right), \tag{B 13b}$$

where the factor $\alpha(\bar{h}_1 - h_{1b})\,\bar{h}_1$ (α is a small number) guarantees that the disturbance is weaker than the vortex at all points). α was chosen such that the velocity of the disturbance would be 10 times weaker than that of the vortex:

$$\frac{\max u'}{\max \bar{u}} = 0.1.$$

Typically, α was in the range 0.01–0.04 (see table 1).

Formulae (B 12)–(B 13) determine the initial condition for the disturbance. It can be demonstrated that it contributes to all azimuthal modes and is thus sufficient to comprehensively test the stability of the vortex.

REFERENCES

Benilov, E. S. 1993 Baroclinic instability of large-amplitude geostrophic flows. *J. Fluid Mech.* **251**, 501–514.

Benilov, E. S. & Reznik, G. M. 1996 The complete classification of large-amplitude geostrophic flows. *Geophys. Astrophys. Fluid Dyn.* **82**, 1–22.

Boyd, J. P. 1983 The continuous spectrum of linear Couette flow with the beta effect. *J. Atmos. Sci.* **40**, 2304–2308.

Butler, K. M. & Farrel, B. F. 1992 Three-dimensional optimal perturbations in viscous shear flows. *Phys. Fluids* A **4**, 1637–1650.

Dewar, W. K. & Killworth, P. D. 1995 On the stability of oceanic rings. *J. Phys. Oceanogr.* **25**, 1467–1487.

Dikiy, L. A. 1976 *Hydrodynamic Stability and Dynamics of the Atmosphere*. Gidrometeoizdat, Leningrad (in Russian).

Farrel, B. F. 1982 The initial growth of disturbances in a baroclinic flow. *J. Atmos. Sci.* **36**, 1663–1686.

Farrel, B. F. 1984 Modal and nonmodal baroclinic waves. *J. Atmos. Sci.* **41**, 668–673.

Farrel, B. F. 1985 Transient growth of baroclinic waves. *J. Atmos. Sci.* **42**, 2718–2727.

Farrel, B. F. 1987 Developing disturbances in shear. *J. Atmos. Sci.* **44**, 2191–2199.

Farrel, B. F. 1988 Optimal excitation of perturbations in viscous shear flow. *Phys. Fluids* **31**, 2093–2102.

Farrel, B. F. 1989 Optimal excitation of baroclinic waves. *J. Atmos. Sci.* **46**, 1193–1206.

Flierl, G. R. 1988 On the instability of geostrophic vortices. *J. Fluid Mech.* **197**, 349–388.

Gustavsson, L. H. 1991 Energy growth of three-dimensional disturbances in plane Poiseuille flow. *J. Fluid Mech.* **224**, 241–260.

Helfrich, K. R. & Send, U. 1988 Finite-amplitude evolution of two-layer geostrophic vortices. *J. Fluid Mech.* **197**, 331–348.

Killworth, P. D. 1980 Barotropic and baroclinic instability in rotating stratified fluids. *Dyn. Atmos. Oceans* **4**, 143–184.

Lai, D. Y. & Richardson, P. L. 1977 Distribution and movement of Gulf Stream rings. *J. Phys. Oceanogr.* **7**, 670–683.

Olson, D. B. 1991 Rings in the ocean. *Ann. Rev. Earth Planet. Sci.* **19**, 283–311.

Orr, W. M. F. 1907 The stability or instability of the steady motions of a perfect liquid and of a viscous liquid. Part II: A viscous fluid. *Proc. R. Irish Acad.* A **27**, 69–138.

Paldor, N. & Nof, D. 1990 Linear instability of an anticyclonic vortex in a two-layer ocean. *J. Geophys. Res.* **95**, 18,075–18,079.

Phillips, N. A. 1954 Energy transformation and meridional circulation associated with simple baroclinic waves in a two-level, quasi-geostrophic model. *Tellus* **6**, 273–286.

Ripa, P. 1997 Instability of a solid-body rotating vortex in a two-layer model. *J. Fluid Mech.* **242**, 395–417.

Ripa, P. 1998 A low-frequency one-layer model with variable stratification and vertical shear. *J. Fluid Mech.* to appear.

Tai, C.-K. & Niiler, P. P. 1985 Modeling large-scale instabilities in the Kuroshio extension. *Dyn. Atmos. Oceans* **9**, 359–382.

Young, W. 1994 The subinertial mixed layer approximation. *J. Phys. Oceanogr.* **24**, 1812–1826.